

Carit Martin Brødsgaard Hansen

**A NEW MICROFLUIDIC PLATFORM FOR CONFINEMENT OF SINGLE
MICROPARTICLES IN FREE SOLUTION**

MASTER'S DEGREE FINAL PROJECT

supervised by Prof Jaume Massons

MASTER'S DEGREE IN NANOSCIENCE, MATERIALS AND PROCESSES



UNIVERSITAT ROVIRA I VIRGILI

Tarragona

2011

A new microfluidic platform for confinement of single microparticles in free solution

Carit Martin Brødsgaard Hansen

Master's Programme in Nanoscience, Materials and Processes: Chemical Technology at the Frontier, 2015-2016

e-mail: carit.brodsgaard@urv.cat

Supervisor: Jaume Massons

Física i Cristal·lografia de Materials i Nanomaterials (FiCMA-FiCNA), Departament de Química Física i Inorgànica, Universitat Rovira i Virgili, Campus Sescelades, c/ Marcel·lí Domingo, s/n. 43007 Tarragona, Spain.

Abstract

Studying microparticles on an individual level can provide much greater levels of detail than when studying microparticles in batches. Various platforms and methods now exist for studying particles individually, but because these, one way or another, affect the integrity of the particle, they are particularly problematic to use for studying biological cells, which generally are very sensitive by nature. In this project, a proof of concept is demonstrated for a new microfluidic platform that can be used to trap a single particle and subsequently position the particle so that it does not come into contact with anything other than the fluid inside the microfluidic chip. The system consists of: a microfluidic chip of poly(dimethyl)siloxane (PDMS) in which particles will enter and be controlled, a pressure controller which generates the pressures for controlling the flow of fluid, a microscope setup with a camera for observing the particles inside the PDMS chip and a software for tracking and controlling the position of a particle. The achievement of successfully confining a microparticle in free solution supports the further testing and development of the platform towards making a system which enables automatic confinement of single cells in free solution, in a way that, in contrast to other methods, leaves the integrity of the cell unaffected.

1. Introduction

Studying microparticles (cells, pollen, synthetic beads, microcapsules etc.) under very simple conditions is fundamental in order to understand how they behave in very complex environments. For example, while the outcome of a given medical intervention may be studied best in a living model, studies on isolated cells generally provide a better opportunity for investigating actual molecular and chemical mechanisms. With conventional methods for studying particles, the problems have however been that multiple parameters are not controllable (Astashkina and Mann, 2012; Bancos *et al.*, 2012) and that the particles may be affected unnaturally by the handling of the particles. For instance, testing the effects of a chemical compound on cells typically involves adding the compound to a well, which contains a solution of a known number of cells. After a given period of time, the effects, for instance the number of cells alive, are compared to a control experiment, where the compound was not added. Such experiment does not enable monitoring of individual particles and so the assay does not take into consideration that cells in the same population may differ in many characteristics. For example, they can have different sizes, be at different

stages of the cell cycle and have replicated a different number of times (Schorl and Sedivy, 2007).

Progress has been made in the development of methods that enable confinement of single microparticles in solution. Snapshot measurements of particles can be made with the technique known as flow cytometry, while more recently developed methods allow assessment of individual particles to be performed continuously. Such methods include tweezing-based confinement methods, which involve selective trapping of a single particle in an applied field of energy, where the applied energy can be in the form of optical, acoustic, magnetic or electrical potential energy (Neuman and Block, 2004; Gosse and Croquette, 2002; Hertz, 1995; Lungu *et al.*, 2015). However, the undesirable consequence of trapping a particle with these methods is that a significant portion of the energy applied will dissipate in the particle, which makes all these methods unsuitable for numerous applications and in particular for use on biological material (Ayano *et al.*, 2006; Rasmussen *et al.*, 2008).

Within the discipline of microfluidics, the ability to trap single particles have been reported with different methods (Lee and Liu, 2015; Benavente-Babace *et al.*,

2014; Khalili and Ahmad, 2015). These methods are based on the trapped particles to be in physical contact with the solid material that makes up the particle trap. Although this removes the need for using an applied energy field, this unnatural contact to the solid trapping structure still compromises the natural integrity of the confined particle. However, it has recently been demonstrated that single microparticles can be confined inside a microfluidic device without the particle being in contact with any solid support (Tanyeri and Schroeder, 2010; Tanyeri and Schroeder, 2013; Shenoy *et al.*, 2015). This can be achieved by confining a particle in a so-called stagnation point, which develops in a four channel junction where two opposing flows of fluid meet and exit perpendicularly through two other channels. However, with this method, it is currently not possible to monitor if a confined particle comes into contact with the floor or the ceiling of the microfluidic channels, nor to efficiently guarantee that it does not occur.

It should also be mentioned that single particles also have been confined inside microfluidic devices by means of noncontact mechanisms that involve the formation of microvortices (Lutz *et al.*, 2006; Petit *et al.*, 2012). Extensive swirling of a particle is however problematic since it can cause undesirable effects and also may complicate the process of analysing the trapped particle.

With no methods existing that enable individual particles to be studied without affecting the inherent integrity of the particles, it is not possible to perform truly reliable experiments on particles. For this reason, I propose a microfluidic platform that allows single microparticles to be manipulated and analysed continuously in free solution inside a microfluidic chip. Importantly, this is achieved without the need for the particles to be subjected to any pre-modification or applied energy field that adversely will affect their inherent integrity.

The microfluidic platform that I present has some similarity with the system presented by Tanyeri and colleagues, in that it is composed of four channels that all intersect at a junction, where the single particle confinement will take place. An important difference is however that, in one of the channels, a barrier is placed, which has a narrow hole in its centre that can capture a particle that is too large to pass through the gate hole. By controlling the flow inside the microfluidic chip, the particle can be pushed back into the four channel junction and be confined while it is in free solution.

The microfluidic platform presented here has a range of potential applications and advantages for a variety of studies. For example, it can potentially be very useful for performing highly reliable studies on the effects of various chemical agents on cells, or for studying the response of microcapsules, when they are exposed to various

intensities of light. Another important advantage of this microfluidic platform is that a cell potentially can be kept away from the other cells of the solution, as well as the substances that they may secrete (Tumarkin *et al.*, 2011). On this basis, the microfluidic platform presented has a potential to become a useful tool for generating highly reliable and accurate information on microparticles, which ultimately could lead to significant improvements in relation to microparticle manipulation, disease diagnosis and faster development of new and more effective medical therapies.

2. Methods and procedures

A range of fabrication, experimental and computational methods and procedures have been carried out for this project. These are described in this section.

2.1. The platform setup

The entire platform was set up according to the diagram in figure 1A. A microfluidic chip of PDMS, for the particles of interest to flow through, was mounted on a moveable stage (ThorLabs), where a light source below could pass light through the microfluidic chip and into a 4x magnifying objective, from where the light was guided to a uc400 camera (ThorLabs). The camera was capable of capturing video at a frame rate of up to 30 frames per second and was connected to a laptop computer (Satellite M50-A-11E, Toshiba), from where it was possible to control the individual pneumatic pressures applied to four liquid containers by the OB1 Mk3 pressure controller (Elveflow). In response to the pressures being applied, fluid would move between the liquid containers and the channels of the microfluidic chip via microfluidic tubes.

2.2. The microfluidic chip design

The chip was designed to consist of 4 channels, x_1 , x_2 , y_1 and y_2 , that all intersect at a junction as shown in figure 1B. Channels y_1 and y_2 were designed to each have a channel length of 25.0 mm with a 90° turn occurring 10 mm away from the four channel junction. Channels x_1 and x_2 were designed to be straight channels, both with a channel length of 15 mm. In contrast to the other channels, channel x_2 was designed to have a slot near to the four channel junction for holding a barrier that will play an essential role in trapping and confining single particles. By inserting a barrier which has a narrow hole through the centre, a particle with a diameter larger than the hole will be unable to pass the barrier and will instead be trapped in front of the hole and block the flow. A subsequent reversion of the flow direction, will then push the trapped particle away from the barrier and back into the four channel junction, where the particle will be in contact with nothing else but the fluid. The particle can then be confined within the area of the four channel

junction by carefully adjusting the individual pressures applied to the four microfluidic channels.

For the proposed design, the fluid dynamics in the four channel junction was computer simulated using COMSOL (see supplementary information). This simulation supported the possibility of generating a point (a stagnation point) in front of the gate, where the opposing pressures cancel each other out to generate a tiny point where fluid movement is very slow (figure 2).

2.3. The microfluidic chip fabrication

The fabrication of the entire microfluidic chip involved several processes including photolithography, soft lithography, careful insertion of a gate of SU-8 into the microfluidic chip and plasma oxidation for sealing together two pieces of PDMS.

2.3.1. Photolithography

Photolithography is a common technique used in the development of microfluidic devices (Sia and Whitesides, 2003) and was carried out for two purposes: for making the mould used for making microfluidic channels in PDMS (wafer 1) and for making gates of SU-8 that could be inserted into the chip (wafer 2). In both cases, a silicon wafer was first polished and cleaned with ethanol and then blow dried with nitrogen gas to remove the ethanol.

1 ml of adhesion promoter, OmniCoat™ (from Microchem), was applied to wafer 1 but not to the other, since it on wafer 2 could complicate the later process of detaching the fabricated gates from the silicon wafer.

To both wafers was applied 1 ml of SU-8, a resin commonly used as a negative resist in photolithography (del Campo and Greiner, 2007). To make the layer of SU-8 thin and uniform, the wafers were spun around their own centre, first at 1500 rotations per minute (rpm) for 10 seconds after which wafer 1 was spun at 2800 rpm for 40 seconds, while wafer 2 was spun also for 40 seconds but at 8000 rpm instead, in order to produce a thinner SU-8 resist layer. Both wafers were soft baked at 100 °C for 60 minutes. The resist that had build up at the outer rim of the wafers, due to the surface tension of the resist, was removed by carefully applying a total of 3 ml of the edge bead remover, AZ® EBR Solvent (Clariant GmbH) to the outer edge, while spinning the wafer at 500 rpm.

In an MG 1410 mask aligner, a chromium photo mask, was placed directly on top of the SU-8 resist-covered silicon wafers. The photo mask carried the design of the microfluidic structures, specified for the chip, as the only area not covered by chromium. For each of the wafers, a photolithographic exposure was carried out for 4 seconds, with ultraviolet light at wavelengths between 365 nm and 405 nm. After the exposure, the photo mask was removed and the wafer was heated at 65 °C for 3 minutes on a hot plate and at 100 °C for an additional

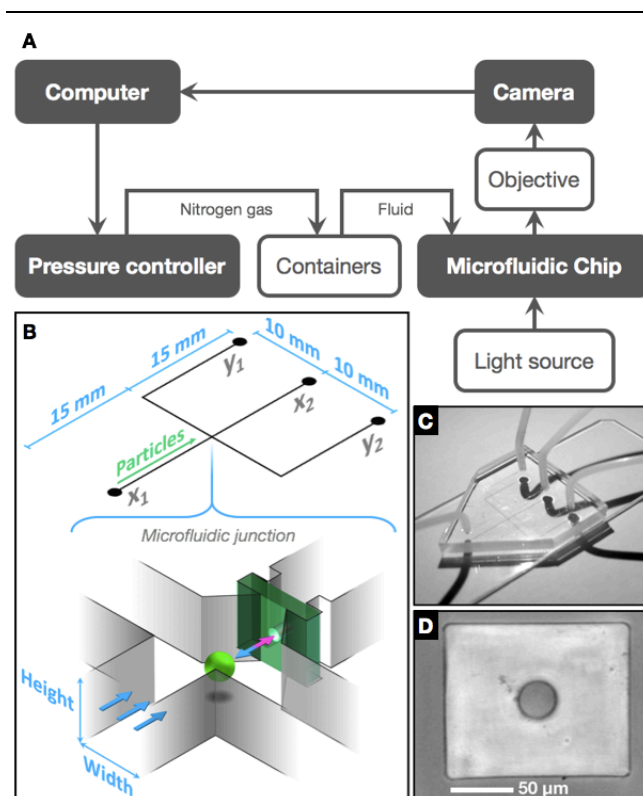


Figure 1. A) Diagram of the setup used for controlling the flow of fluid inside the microfluidic chip. B) Illustration of the microfluidic design including an enlarged view of the four channel junction. C) Photo of the fabricated microfluidic chip of PDMS placed on a microscope glass slide, where tubes have been connected. D) Microscopic image of the gate of SU-8 before it was fitted into the specified slot in the microfluidic chip.

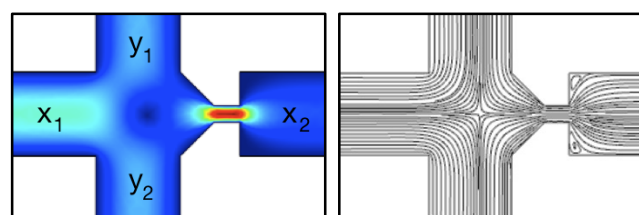


Figure 2. Computer simulations of the fluid dynamics at the four channel junction, showing how high pressure applied to left and right channels (x_1 and x_2) lead to the generation of a stagnation point, where the flow is very slow, in the four channel junction. Left diagram shows flow velocities with low to high flow velocities indicated by dark blue and red respectively. Right diagram indicates streamlines.

7 minutes.

Finally, to remove the unwanted, unexposed areas of SU-8, the wafers were swirled around in a petri dish containing AZ® EBR Solvent until all unexposed SU-8 had been removed. Ethanol was then used to rinse the wafers to prevent any potential further etching of the remaining exposed SU-8.

2.3.2. Soft lithography (replica moulding)

The microfluidic chip was made in poly(dimethyl)siloxane (PDMS) primarily because it is an affordable, transparent and gas-permeable polymer, which commonly is the preferred choice of material for microfluidic chips due to its various excellent properties (McDonald and Whitesides, 2002). It was made using the soft lithography method, specifically known as replica moulding (Sia and Whitesides, 2003), where the wafer (wafer 1), which had been prepared by the technique of photolithography to have raised structures of SU-8 on top of it, was used as a mould for making an imprint of the desired microfluidic structures in PDMS.

The PDMS (Sylgard® 184, from Dow Corning) was prepared by mixing the monomer and curing agent in a 10:1 weight ratio, according to the instructions of the supplier. The mixture was then mixed thoroughly and degassed in cycles of vacuum. Then it was poured into a dish of folded aluminium foil, where the ready mould (wafer 1) had already been placed, facing up. After 24 hours of allowing the PDMS to polymerize and to degas on top of the wafer in an oven at 80° C, the aluminium foil dish was peeled off and the solidified PDMS was removed from the mould. The PDMS was then cut to fit on a glass slide, while the mould was saved so that it could be reused to make replicas of the microfluidic PDMS chip, should it be necessary. In addition, the PDMS mixture was also used to make a cover piece of PDMS that would be used to cover the side of the PDMS base piece that contained the microfluidic structures.

2.3.3. Preparation of SU-8 gates

To serve as gates, rectangles with a hole in the middle, were fabricated in SU-8 as described in the section on photolithography. After the process of photolithography was completed and unexposed SU-8 had been removed, the wafer was placed in a petri dish containing ethanol. A plastic pipette was then used to move the liquid in the proximity of the SU-8 structures up and down, in order to release the SU-8 structures from the wafer. The SU-8 structures were then collected with the pipette and transferred to a glass slide to dry. A regular plastic pipette was found to be a more convenient tool than a pipette of glass, as the SU-8 gates had a tendency to stick to the inside of the glass pipette.

2.3.4. Insertion of SU-8 gate

Under a microscope, a suitable SU-8 gate was identified from the glass slide on which the fabricated gates were stored. The chosen SU-8 gate was then moved to the PDMS base using a tool that had a fine tip. Through different tries, it was found that a tip of a plastic material was more convenient for manoeuvring the SU-8 gate than a tip made of glass, metal, wood or a piece of hair. Once

placed on the PDMS base, the same tool was used to push the SU-8 gate by hand towards the designated slot in the PDMS. Ultimately, with some delicate manoeuvring the SU-8 gate was successfully inserted into the chip.

2.3.5. Bonding together the two pieces of PDMS

With the SU-8 gate in place in the PDMS base, the PDMS base and top cover were moved to a reactive ion etching apparatus (Oxford Instruments), where a plasma of reactive oxygen was produced for 20 seconds to modify the surface of the PDMS. The base and top pieces of PDMS were then quickly put into contact with each other and due to the surface activation by the oxygen plasma, the two pieces became irreversibly sealed to each other through the formation of covalent bonds (McDonald *et al.*, 2000). Finally, holes were drilled in the PDMS cover so that tubes could be inserted into the microfluidic chip and thus enable fluid to enter the microfluidic channels.

2.4. Confocal imaging characterization

The size dimensions of the microfluidic channels and the gates of SU-8 and their hole diameter were identified using an optical confocal profiler (PLμ 2300, Sensofar). Measurements were made using x- and y-coordinates with the microscope in regular microscopic mode, whereas interferometry mode was used to locate the position of surfaces and to measure the distance between them using z-coordinates.

2.5. Preparation of particles

In this project, the model particle used were synthetically produced green fluorescent polystyrene microbeads with an average diameter of 40 μm ($2.91 \cdot 10^5$ microbeads per ml, density 1.06 g/cm³, Phophorex). These microbeads were specifically chosen due to their great morphological stability, their size which is comparable to that of large biological cells, and their fluorescence, which makes it possible for the particle tracking software developed to correctly identify the particle. According to the supplier, the fluorescence of the microbeads was excitable by blue light, peaking at a wavelength of 450 nm, which consequently will result in the emission of green light, peaking at a wavelength of 500 nm.

The fluorescent microbeads were added in a 1:51 ratio to a suspension of 1:5 solution of glycerol in deionized water, where the glycerol served to increase the density of the suspension so that it would approximate the density of the microbead suspension.

2.6. Pressure control

The flow of fluid inside the microfluidic chip was controlled by applying different amounts of pressure to each of the four channels of the microfluidic chip using a piezoelectrically controlled OB1 Mk3 pressure controller

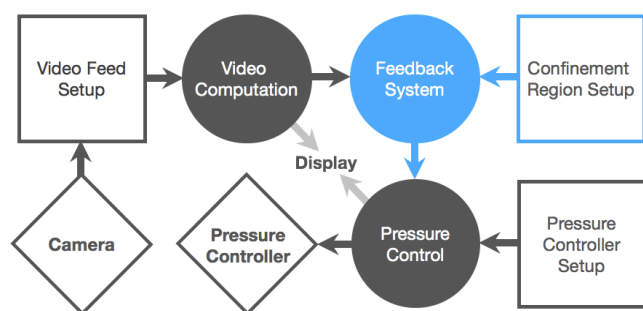


Figure 4. Flow diagram of the software, developed for tracking and confining a particle in free solution.

(Elveflow). Through an inlet, nitrogen gas was introduced at a pressure of 2 bar to the pressure controller and distributed to four outlets, which each were connected to one of four liquid containers through 125 cm long tubes that had an internal diameter of 2,38 mm (Elveflow). In response to pneumatic pressures being applied to the liquid containers, fluid would move, from inside the liquid container, to the channels of the microfluidic chip, via 30 cm long tubes of polytetrafluoroethylene (PTFE), which had an internal diameter of 0.79 mm (Elveflow). The outlet of the pressure controller connected to the x_1 microfluidic channel, was capable of providing a pneumatic pressure of up to 200 mbar, while the outlet connected to channel x_2 could provide 2000 mbar and the outlets connected to channels y_1 and y_2 , each could deliver a pressure of up to 1000 mbar.

2.7. The software

The initial preliminary tests on the performance of the setup and the chip, was carried out by controlling the OB1 Mk3 pressure controller (Elveflow) with the software Elveflow SI (version 2.6.1). This software works well for controlling the pressure controller but with the intention to build an automated feedback system which is based on particle tracking, it was found to be inadequate for that. To make an automated feedback system, I therefore developed a new software, Autofluidics, with the necessary features for that (see figure 4 and supplementary information). This was achieved using LabVIEW and with a virtual instrument developed by Elveflow for interacting with their OB1 Mk3 pressure controller and another virtual instrument from ThorLabs for interacting with their uc400 camera.

2.7.1. Pressure control modes

The control module of Autofluidics was built to enable the OB1 Mk3 pressure controller to be operated at different modes and using different sets of pressure. Thanks to this, static pressures could be applied to all four

channels, while the pressure to channel x_2 also could be adjusted according to an amendable sinus curve. Also, important for making automated particle confinement possible, the pressures to channels x_2 and y_1 could be set to be adjusted automatically according to the settings in the feedback module. Moreover, a set of pressures could be chosen using a drop down menu and the inclusion of a cycle feature made it possible to set up the system to automatically cycle, at defined intervals, between different modes and pressure sets.

2.7.2. Video computation

The Autofluidics software obtains a video feed from the uc400 camera, and enables settings, such as the capturing rate and the exposure time, to be adjusted. The software then performs computation on the video feed to generate a binary copy of it. In the binary video, a pixel can only be black or white and will depend on the light intensity of the corresponding pixel in the original video feed and an adjustable threshold. Some additional computation is performed on the binary video to count the number of pixels that are both right next to each other and also above the specified threshold value. This enables a cluster of pixels to be located and characterised as one single unit, which is useful for identifying a particle from potential noise pixels. Ultimately, the video computation will generate information on the size of an area of pixels that are above the threshold as well as the coordinates of the centre of that area of pixels.

In order for the feedback system to assess whether the centre of the particle is inside or outside a desired area, a graphical overlay is placed on top of the video feed, where the top, bottom, left and right borders of a desired confinement area can be set easily.

2.7.3. Feedback module

Once the pressure control mode is set to “Confine” and the feedback module is activated, the Autofluidics software will analyse if the particle (i.e. the coordinates of the centre of the pixel area that was found through the video computation module to represent a particle) is situated within the desired confinement area. If the coordinates are found to be situated to the left or right of the desired area that has been set, the pressure in channel x_2 will change to bring the particle into the desired area. Likewise, if the coordinates are over or under the area, the pressure applied to channel y_2 will change. For avoiding feedback overcompensation, the feedback module only compares the position of the particle and the borders of the defined confinement area at adjustable intervals of time. For this reason, the duration of pressure changes, prompted by the feedback, is adjustable as well and also it will be influenced by how far the particle centre is away from the defined confinement area.

2.8. Flow resistance of channels

Due to the channels of the microfluidic chip being very narrow, the microfluidic chip exerts a substantial amount of resistance to the flow that passes through it. Flow resistance is therefore an important parameter and important for understanding the behaviour of the flow inside the chip. By determining the volume flow rate, Q , at different hydraulic pressures, P_H , the hydraulic flow resistance, R_H , is given by:

$$R_H = \Delta P_H / Q \quad (\text{Eq. 1})$$

where ΔP_H is the difference in the hydraulic pressure. R_H depends on the dimensions of a channel (height, width and length) and the physical parameters of the fluid (viscosity). For a rectangular channel, where height > width, R_H is given by:

$$R_H = \frac{12}{(h/w)^{-0.63}} \frac{\eta L}{w^4} \quad (\text{Eq. 2})$$

(Bruus, 2008) where η is the dynamic viscosity of the fluid in $\text{Pa} \cdot \text{s}$ and h , w and L are the height, width and length of the channel respectively in m. The values of R_H are then given in $\text{Pa}/\text{m}^3/\text{s}$.

To find the flow resistance of each channel, the flow was directed through two chosen channels at a time according to the diagram in figure 5A by selectively blocking the other two channels. A flow sensor (MFS2 from Elveflow) was used to obtain the flow rate measurements at different pressures (figure 5B) and was placed in the connection between the pressure controller and the microfluidic chip. The flow sensor had an internal diameter of 150 μm and had a capability to measure flow rates in the range from 0.4 to 7.0 $\mu\text{l}/\text{min}$. This range was sufficient for obtaining a linear behaviour of the flow resistance, although the microfluidic system could be operated at higher flow rates for other purposes.

Deionised water was used as fluid and had to be able to exit the chip freely. Unfortunately, this caused a droplet to evolve on top of the exit, which inflicts an overpressure to the fluid which changes according to the droplet size. However, by obtaining the flow rate measurements, not before a droplet had grown to have a radius of 3 mm, the change in internal pressure of the droplet became small enough so that the effects of the droplet could be discarded (see supplementary information).

Also, the results were influenced by the hydraulic flow resistance, not only from the microfluidic chip, but also from the background resistance provided by the tubing and the flow sensor itself. However, note that from equation 1, it is the change of pressure, ΔP , and not the actual value of the pressure that is required for finding the flow resistance. Therefore, one test was performed, where

the microfluidic chip was disconnected from the setup and allowed the background resistance from this test to subsequently be subtracted from all of the measurements.

Since changes in the setup, e.g. elevation or tube bending, could affect the measurements, the entire setup was fixed to ensure that the path of the fluid, from the liquid container to the microfluid chip, was not altered.

2.9. System response characterization

Using the developed software, Autofluidics, a particle was captured inside the microfluidic chip, in front of the inserted gate. In "Manual" mode, the sinus curve profile mode was activated for channel x_2 , and the pressures of all of the channels were equilibrated so that the trapped particle, would move straight to the centre of the microfluidic junction and back again every 1.5 seconds. When the setup was balanced, the setting was used as a reference for changing different individual parameters. The subsequent behaviour of the single particle was video recorded using the uc400 camera (Thorlabs) and was analysed with the free and widely used imaging software, ImageJ (Schneider *et al.*, 2012), using the plugin, Manual Tracking, to determine changes in the position of the particle over time.

3. Results and discussion

3.1. Characterization of the microfluidic chip

The channels of the microfluidic chip were determined with a confocal profiler to have a height of 114 μm and a width of 109 μm . The gate inserted into the PDMS chip measured 147 μm by 125 μm and had a thickness of 42 μm and a hole with a diameter of 28 μm through the centre (see the microscopic image in figure 1D). Being 11 μm taller than the microfluidic channels, the gate was large enough to be in sufficient contact with both the top and bottom of the microfluidic channel and since PDMS exhibits great elasticity (Wang *et al.*) the gate did not appear to compromise the sealing of the PDMS.

3.2. Flow resistance

For different flow paths (figure 5A), the fluid flow rates, obtained at different pressures, are presented in figure 5B. The results very clearly show linear tendencies and the fact that all of the tendency lines intersect each other, close to perfectly, at a flow rate of 0.0 $\mu\text{l}/\text{min}$, verifies that the setup was indeed kept very stable throughout the course of obtaining the measurements. For maintaining a flow rate of 0.0 $\mu\text{l}/\text{min}$, a pressure of approximately 10 mbar was required for this particular setup, but this pressure value was mainly a result of the gravitational force acting upon the fluid and will change depending on how the system is setup. Indeed, during preliminary setup tests, it was noticed that changing the vertical position of the microfluidic chip relatively to the rest of the system,

affected the amount of pressure that was needed to produce a given flow rate. For that reason, it was ensured that the chip in the setup was horizontally levelled and was elevated high enough so that the pressure needed for maintaining a flow rate of 0 $\mu\text{l}/\text{min}$ had to be positive.

Based on the flow rate measurements, the flow resistance of all of the fluidic paths were calculated using equation 1. After adjusting for the background resistance of the setup, the resistances of paths A, B, C and D were calculated to be: $R_A = 1.26$, $R_B = 1.59$, $R_C = 11.35$ and $R_D = 11.35$ mbar/ $\mu\text{l}/\text{min}$ respectively. On the assumption that the channels maintained their resistance irrespective of the path, the flow resistance of each channel could be calculated from the flow resistances of the different paths, the following way:

$$R_{x_2} = (R_C + R_D - R_B) / 2 = 10.55 \text{ mbar}/\mu\text{l}/\text{min}$$

$$R_{y_1} = (R_C + R_B - R_C) / 2 = 0.80 \text{ mbar}/\mu\text{l}/\text{min}$$

$$R_{y_2} = (R_D + R_B - R_C) / 2 = 0.80 \text{ mbar}/\mu\text{l}/\text{min}$$

$$R_{x_1} = (R_A - R_{x_2}) = 0.46 \text{ mbar}/\mu\text{l}/\text{min}$$

where R_{x_1} , R_{x_2} , R_{y_1} and R_{y_2} , are the resistances of channels x_1 , x_2 , y_1 and y_2 respectively. These results (displayed in figure 5C) are in fair agreement with the values which can be found through numerical calculations using equation 2. With $\eta = 1 \text{ Pa} \cdot \text{s}$, equation 2 gives that a rectangular channel with $w = 109 \mu\text{m}$, $h = 114 \mu\text{m}$ and with the length, $L = 2.5 \text{ cm}$ (true for channels y_1 and y_2) will have a flow resistance of $5.11 \cdot 10^{12} \text{ Pa}/\text{m}^3/\text{s}$, or $0.85 \text{ mbar}/\mu\text{l}/\text{min}$. When $L = 1.5 \text{ cm}$ (true for channel x_1), the resistance is instead calculated to be $0.51 \text{ mbar}/\mu\text{l}/\text{min}$.

In contrast to the other channels, equation 2 is not applicable to channel x_2 , as the channel cannot be considered to have a simple geometric shape. It includes an irregular section with a gate and structures for holding the gate that complicate the possibility of calculating the total flow resistance. Nonetheless, the experimental results indicate that the gate inserted into channel x_2 was responsible for a substantial constriction of flow, which resulted in that channel having a total resistance that was much greater than that of the other channels. Comparing to channel x_1 , which had the same length, but in contrast did not contain a gate, channel x_2 had a 25-fold higher resistance.

With regards to the relationship between channels, the flow resistance of channel x_1 , being 0.60 of the length of channel y_1 and y_2 , it is also in agreement that the experimental flow resistance of channel x_1 is 0.575 that of channels y_1 or y_2 . Finally, due to this good correlation between the experimental and numerical results, it can be stated with good certainty, based on the channels x_1 , y_1 and y_2 , that the resistance of the microfluidic channels of the chip were $0.32 \text{ mbar}/\mu\text{l}/\text{min}$ per cm length of regular microfluidic channel.

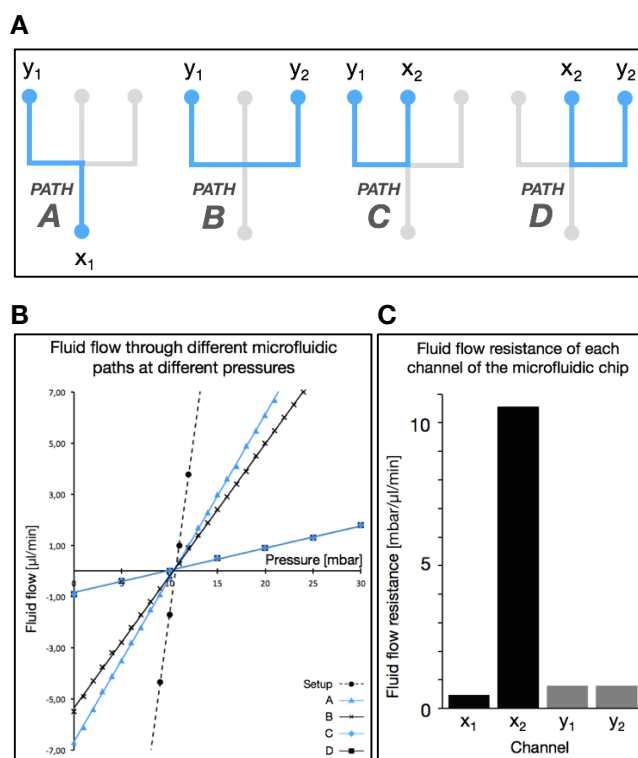


Figure 5. A) Diagram of the setup for finding the flow resistance of the channels of the microfluidic chip. B) Plot of the flow rate values recorded at different applied pressures for different paths (A-D) through the chip, except for the curve, “Setup”, where the microfluidic chip was disconnected. C) The hydraulic flow resistance calculated for each channel of the microfluidic chip.

3.3. Characterization of the response of the platform

By capturing a particle in front of the gate and using the Autofluorescence software to apply an oscillating pressure with a sinus curve profile, to channel x_2 , as illustrated in figure 6A, multiple aspects of the complete system could be evaluated. It was found that not only the maximum set pressure of the pressure oscillation, but also the minimum pressure and the wave period, had an effect on how far the particle moved away before returning to the trapped position. From figure 6B it appears that the wave period of the pressure oscillation has some influence on the maximum particle displacement, but also that at longer wave periods this diminishes. Measurements at wave periods shorter than 0.8 s were not found to be reliable.

When keeping the period and the maximum set pressure constant for the oscillation and varying only the minimum set pressure, it can be seen in figure 6C that there was an optimum in particle movement, when the set pressure oscillated over a pressure range of about 4.5 %. For these experiments, a 4.5 % pressure difference was equivalent to 7.4 mbar. Particularly, for a set pressure oscillating with a wave period of 1.5 seconds over this pressure range of 7.4 mbar, the surprisingly long particle

trajectories is an indication that a significant overcompensation of the pressure must be taking place. This is most likely caused mainly by the OB1 Mk3 pressure controller, as such an effect of overshooting the set values is common for a proportional–integral–derivative (PID) controlled device (Skoczowski *et al.*, 2005). This also explains why particle movement could be observed even when the maximum pressure was slightly smaller than the pressure needed to release the particle with static pressure.

At set pressure ranges greater than 7.4 mbar, the length of the particle trajectories again shortened, which likely was due to the range becoming too great for the requested maximum pressure to be reached in the short periods of 1.5 seconds.

Based on these findings, it has been learned that large rapid changes in the set pressures likely will lead to the pressure controlling equipment initially applying inaccurate pressures. For some purposes, it may therefore be best to make small incremental adjustments when the pressure adjustment has to be made sensitively.

3.3.1. Responsiveness

Another observation was made on the responsiveness of the developed system. With a single particle captured and by applying a sinus curve profile to the pressure control of channel x_2 , it was found that, when using the Autofluiddics software, the frequency of particle movement would not correspond to the periods of the applied sinus curve when the period became shorter than 0.8 seconds. This is interesting because the frequency of particle movement would correspond to periods as short as 0.4 seconds when the Elveflow SI software was used. This difference may either be due to the various memory demanding modules of Autofluiddics, slowing down the processing speed of the computer, or because there is a delay in the process of transferring the pressure values from Autofluiddics through the virtual instrument that relays the values to the OB1 Mk3 pressure controller.

3.4. Confinement of single particles in free solution

Being able to confine single particles in free solution, without affecting their integrity, was a huge challenge and was a great motivational factor for starting this project. I can here report that confinement of a single microparticles was achieved with the microfluidic platform developed. The confinement was made by controlling the pressures applied to the four channels of the microfluidic chip and could be achieved by making the pressure adjustments manually (figure 7A) and also it was achieved by using the automated feedback system included in the developed Autofluiddics software. For both manually and automatically controlled confinement, it has been possible to sustain the confinement for more than a minute. So far, with the feedback module not fully

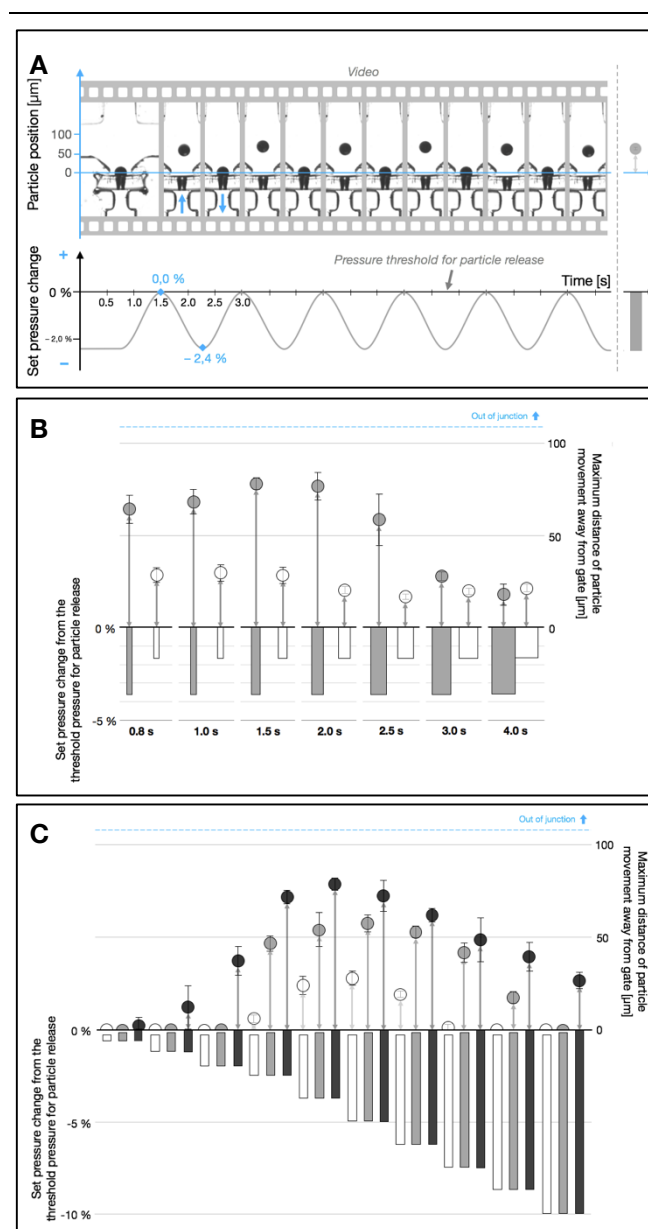


Figure 6. Movement of the particle away from the trapped position (reference position), when pressure, oscillating according to a sinus curve profile, is applied to channel x_1 . A) Snapshots of particle position when at minimum and maximum distance to the reference position, while the set pressure to channel x_1 oscillates. B) The maximum particle movement in response to the set pressure applied to channel x_1 at different periods of oscillation. C) The maximum particle movement in response to the set pressure applied to channel x_1 oscillating at ranges with different minimum and maximum values.

developed, the steadiest confinement has been achieved using manually controlled confinement. However, with automatically controlled confinement, particles have been fairly well confined inside the four channel junction, especially in the direction along the x_1 and x_2 channels (x -direction), with the confinement being within approximately 20 µm.

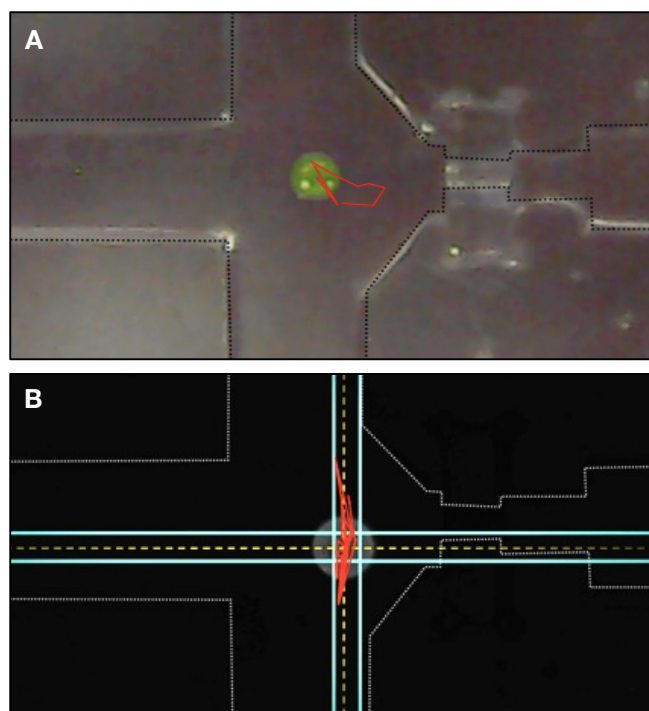


Figure 7. Confinement of single particles in free solution. Particle path (red line) obtained for 1 minute of confinement A) Confinement of particle by manual pressure adjustments. B) Confinement of particle by automatic adjustments based on a predefined desired confinement region and the feedback module of Autofluidics. The dashed yellow lines indicate the centre of the particle,

Because the confined particles had a diameter of about one third of the width or height of the microfluidic channels, the particle is not only affected by the fluid moving inside the, but the particle itself may likely also affect the flow of the fluid (see supplementary information). In their work, Tanyeri and colleagues have primarily used an experimental setup for confining a particle in a stagnation point, where the particles were very small compared to the microfluidic channels. That makes it possible to neglect the effect that the particles have on the fluid flow. At least with this microfluidic platform, it has thus been shown that larger particles also can be confined in free solution inside a microfluidic chip.

3.4.1. No-flow confinement vs. stagnation point confinement

Confinement of a particle in a very tiny region is very sensitive to any disturbances or disequilibrium in the flows. Particle confinement therefore is dependent on the ability to make continuous adjustments of the applied pressures, irrespective of whether the confinement is achieved in a stagnation point or in a no-flow equilibrium, where pressures may be applied, but no net flow of fluid takes place. Particle confinement in a stagnation point will generally be the least stable of the two methods and

consequently will require the feedback system to be more sensitive and responsive. Whereas no-flow confinement has been performed routinely with the platform developed, it has not yet been achieved to confine a particle in a stagnation point with other than small differences in the pressures between the inlet and outlet channels.

Although it was not really achieved with the current setup, further development on the software may make it possible to achieve confinement of a single particle in a stagnation point. For this it is especially suggested that focus is put on improving the feedback response algorithm

4. Outlook and opportunities

4.1. The software/hardware

Developing the software successfully was not just about being able to build the several needed features into the system. It also required simplifying the computation processes and setting up the system to perform required tasks only when needed. Particularly this needs to be a priority, as it demands a lot of computer memory to capture video at a high frame rate and perform fast video processing while also enabling adjustments to be made by the user in real-time and sending the output to a piece of hardware. Since it is the computer hardware, rather than the pressure controller hardware that seems to be the limiting piece of equipment in the system, it will therefore be useful to further optimise the parts of the software that are very demanding on computer memory or to move the platform to a more powerful computer.

4.2. The platform

An important thing that remain open for future investigation is to clarify for how long, a particle will stay away from being in contact with the channel walls, once it is placed in the confined position. Being able to control the movement of the confined particle in x- and y-directions, it remains to be investigated how a confined particle behaves in the vertical direction (z-direction) as it is possible that it will eventually come into solid contact with the base or top of the microfluidic channel. For assessing this, attempts were made with retrieving microscopic images of the channel junction from aside, but so far this work has not lead to any concluding results. The complication of this is mainly that it is difficult to get anything at an angle of about 45 degrees very close to a junction of straight corners and at the same time that a view of the junction from an angle may be affected by the structures of the junction, e.g. due to distortion by the channel walls, especially at the corners, or due to the inserted gate obstructing the view.

Other potential approaches to solving this could be to perform confocal imaging in order to acquire 2D images in different vertical planes while the particle is positioned

for confinement in free solution. This could however compromise the automated confinement system, which needs to be able to assess the horizontal position of the particle constantly and moreover, achieving both a good spatial and temporal resolution may be difficult with this method.

Modifying the surface of the inside of the PDMS, in particular the top and the base of the channel junction, so that it would generate a signal upon being in contact with the particle, could also be an opportunity. The challenge in that case would be to make sure that such sensing mechanism is very reliable and that signals or the lack thereof can be trusted.

5. Conclusion

By developing a new microfluidic platform, it has been possible to confine single particles in free solution inside a microfluidic chip. This has been achieved with an automated system for which it was necessary to custom-build the software, Autofluidics, which can track a single particle inside the microfluidic chip, and use a feedback system to control the position of the tracked particle by appropriately adjusting the pressures, applied by a pressure controller, to each of the four channels of the microfluidic chip. Characteristics were also gathered about the microfluidic chip, the fluid dynamics and the responsiveness of the pressure controlling system, which can help to direct the further development of the system.

6. Acknowledgement

I would like to thank Jaume Massons and Eric Pedrol for providing guidance on the use of equipment and methods and for being available for advice in various situations.

7. References

- Astashkina, A., Mann, B. and Grainger, D.W., (2012). A critical evaluation of in vitro cell culture models for high-throughput drug screening and toxicity and toxicity. *Pharmacology and Therapeutics*, 134, pp.82-106.
- Ayano, S., Wakamoto, Y., Yamashita, S. and Yasuda, K., (2006). Quantitative measurement of damage caused by 1064-nm wavelength optical trapping of *Escherichia coli* cells using on-chip single cell cultivation system. *Biochemical and Biophysical Research Communications*, 350(3), pp.678-684.
- Bancos, S., Tsai, D. H., Hackley, V., Weaver, J. L., and Tyner, K. M. (2012). Evaluation of viability and proliferation profiles on macrophages treated with silica nanoparticles in vitro via plate-based, flow cytometry, and coulter counter assays. *Nanotechnology*.
- Benavente-Babace, A., Gallego-Pérez, D., Hansford, D., Arana, S., Pérez-Lorenzo, E. and Mujika, M., (2014). Single-cell trapping and selective treatment via co-flow within a microfluidic platform. *Biosensors and Bioelectronics*, 61, pp.298-305.
- Bruus, H., (2008). Theoretical microfluidics. *Oxford University Press*, 18.
- del Campo, A., and Christian G., (2007). SU-8: a photoresist for high-aspect-ratio and 3D submicron lithography. *Journal of Micromechanics and Microengineering*, 17(6).
- Gosse, C. and Croquette, V. (2002). Magnetic tweezers: micromanipulation and force measurement at the molecular level. *Biophysical Journal*, 82(6), pp.3314-3329.
- Hertz, H. (1995). Standing-wave acoustic trap for noninvasive positioning of microparticles. *J. Appl. Phys.*, 78(8), p.4845.
- Khalili, A. and Ahmad, M. (2015). Numerical analysis of hydrodynamic flow in microfluidic biochip for single-cell trapping application. *IJMS*, 16(11), pp.26770-26785.
- Lee, L. and Liu, A. (2015). A microfluidic pipette array for mechanophenotyping of cancer cells and mechanical gating of mechanosensitive channels. *Lab Chip*, 15(1), pp.264-273.
- Lungu, M., Neculae, A. and Lungu, A. (2015). Positive dielectrophoresis used for selective trapping of nanoparticles from flue gas in a gradient field electrodes device. *Journal of Nanoparticle Research*, 17(12).
- Lutz, B., Chen, J. and Schwartz, D. (2006). Hydrodynamic tweezers: 1. noncontact trapping of single cells using steady streaming microeddies. *Analytical Chemistry*, 78(15), pp.5429-5435.
- McDonald, J.C., Duffy, D.C., Anderson, J.R., Chiu D.T., Wu, H., Schueller, O.J.A., and Whitesides, G. (2000). Fabrication of microfluidic systems in poly(dimethylsiloxane). *Electrophoresis*, 21, pp.27-40.
- McDonald, J.C. and Whitesides, G.M., 2002. Poly (dimethylsiloxane) as a Material for Fabricating Microfluidic Devices. *Accounts of Chemical Research*, 35(7), pp.491-499.
- Neuman, K. and Block, S. (2004). Optical trapping. *Rev. Sci. Instrum.*, 75(9), p.2787.
- Petit, T., Zhang, L., Peyer, K., Kratochvil, B. and Nelson, B. (2012). Selective trapping and manipulation of microscale objects using mobile microvortices. *Nano Letters*, 12(1), pp.156-160.
- Rasmussen, M., Oddershede, L. and Siegmund, H. (2008). Optical tweezers cause physiological damage to *Escherichia coli* and *Listeria* bacteria. *Applied and Environmental Microbiology*, 74(8), pp.2441-2446.
- Sia, S. and Whitesides, G., (2003). Microfluidic devices fabricated in poly(dimethylsiloxane) for biological studies. *Electrophoresis*, 24, pp.3563-3576.
- Schorl, C., and Sedivy J. M., (2007). Analysis of cell cycle phases and progression in cultured mammalian cells. *Methods*, 41(2), pp.143-150.
- Schneider, C. A., Rasband, W. S., and Eliceiri, K. W., (2012). NIH Image to ImageJ: 25 years of image analysis. *Nat methods* 9(7), pp.671-675.
- Shenoy, A., Tanyeri, M. and Schroeder, C. (2014). Characterizing the performance of the hydrodynamic trap using a control-based approach. *Microfluidics and Nanofluidics*, 18(5-6), pp.1055-1066.
- Skoczowski, S., Domek, S., Pietruszewicz, K. and B. Broel-Plater, (2005). A method for improving the robustness of PID control, *IEEE Transactions on Industrial Electronics*, 52(6), pp.1669-1676.
- Tanyeri, M. and Schoeder, C., (2010). Hydrodynamic trap for single cells and particles. *Biophysical Journal*, 98(3), p.404a.
- Tanyeri, M. and Schroeder, C., (2013). Manipulation and confinement of single particles using fluid flow. *Nano Letters*, 13(6), pp.2357-2364.
- Tumarkin, E., Tzadu, L., Csaszar, E., Seo, M., Zhang, H., Lee, A., Peerani, R., Purpura, K., Zandstra, P. and Kumacheva, E., (2011). High-throughput combinatorial cell co-culture using microfluidics. *Integr. Biol.*, 3(6), p.653.
- Wang, Z., Volinsky, A., and Gallant, N., (2014). Crosslinking effect on polydimethylsiloxane elastic modulus measured by custom-built compression instrument. *J. Appl. Polymer Science*, 131, p.41050.

SUPPLEMENTARY INFORMATION FOR:

A new microfluidic platform for confinement of single microparticles in free solution

Carit Martin Brødsgaard Hansen

1. Computer simulation of the fluid dynamics inside the microfluidic chip

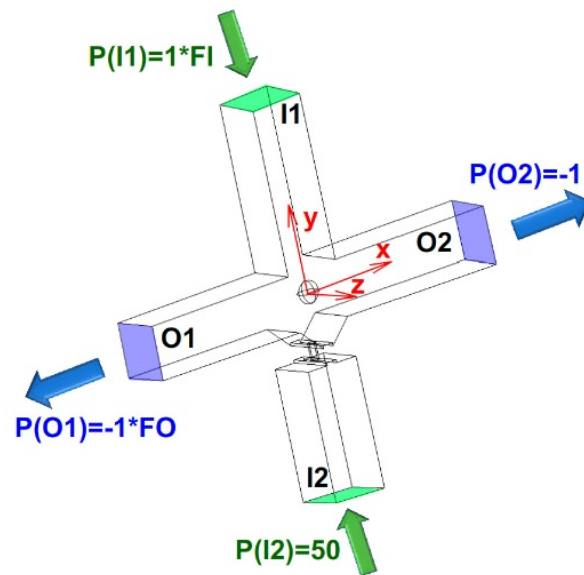
For assessing the behaviour of the fluid inside the microfluidic chip, a three-dimensional computer model was made of the four channel junction and partial differential equations were solved with a 3-D finite-element solver (COMSOL Multiphysics). The geometry of the model is depicted in figure S1 and for mimicking the effect that a particle could have on the fluid flow, a ball-shaped structure was added to the junction of the model. The model was placed so that the junction centre was positioned in the zero coordinate for all three dimensional axes.

To each channel, static pressure was applied and the two factors FI (input factor) and FO (output factor) were introduced to enable a pressure asymmetry to be made between the channels. When both FI and FO equal one, the pressure distribution would become symmetric. Note that a higher base pressure value was applied to input I2, due to the effects of the constricting gate hole. For making the model more realistic, non-slip boundary conditions were included for all the solid boundaries.

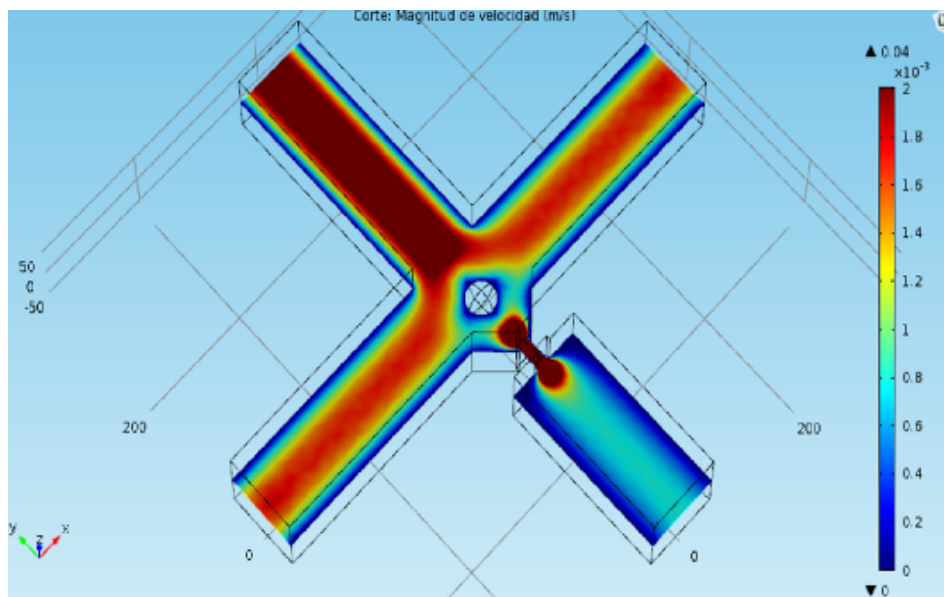
One example of the results obtained is shown in figure S2, which shows the velocity distribution in the $z=0$ plane for $FI=FO=1$ and with the particle located at $(x,y,z = 0,-15,0)$. It is noteworthy that the presence of a particle has a significant effect on the symmetry and velocity of flow in the four channel junction. This was a distortion which increased with the size of the particle. Taking into account that the particle, for each experiment, is immobile, a net force that the fluid impose on the surface can be obtained by surface integration of the stress distribution (computed by the software). For the situation in figure S2, the net force was $(1.27 \cdot 10^{-14}, 5.07 \cdot 10^{-11}, 0)$ N, so mostly a force to push the particle in the positive y -direction, away from the port. Simulations were also carried out with the particle at different positions. The velocity distributions of these simulations are summarized in figure S3.

A parametric study was performed to determine which values of FI and FO that will result in there being no net flow being imposed by the fluid onto the particle when the particle is placed at different positions. With the particle placed at $(0,0,0)$, the optimal value for FI and FO was 1, but at other particle positions the FI and FO values were different. Generally, in order to impose a zero net pressure on the particle it was found that FO had to increase when the position of the particle was moved positively along the x -axis. In other words, when placing the particle closer to the O2 channel, the amount of suction from channel O1, which is determined by FO, had to be increased in order to maintain the particle at the position it was placed. For FI, the inverse was true with regards to the particle position along the y -axis, but similarly it meant that for keeping the particle positioned closer to the I2 channel, FI had to be increased. However, changing any of the factors, FI or FO, affects the fluid velocities of not just only one or two of the channels, but of all four of them. With respect to this, FI and FO should be inversely related to each other and indeed this was found to be the case, as shown in figure S4, where a particle was placed at various positions along the x -axis, while the position along the y - and z -directions was kept at $(0,0)$. It is interesting though that the results of FI and FO were not completely symmetric to each other, which could be due to the channels I1 and I2 not being completely symmetric, since I2 contains a part where the fluid is heavily constricted.

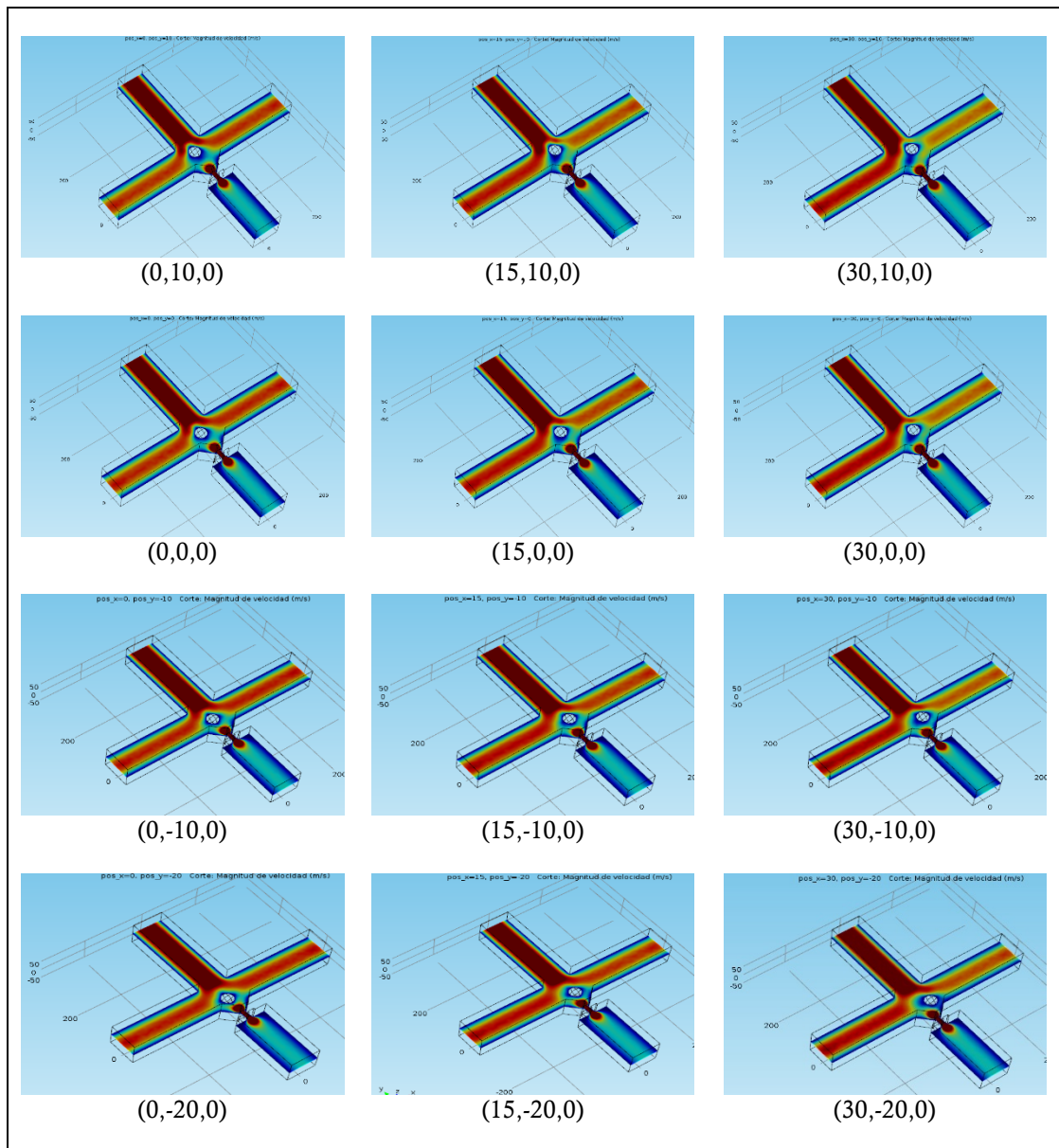
Finally, it was learned from the studies that forces imposed on the particle in the y -direction mainly were affected by changes to FI, while forces imposed in the x -direction mainly were affected by changes to FO.



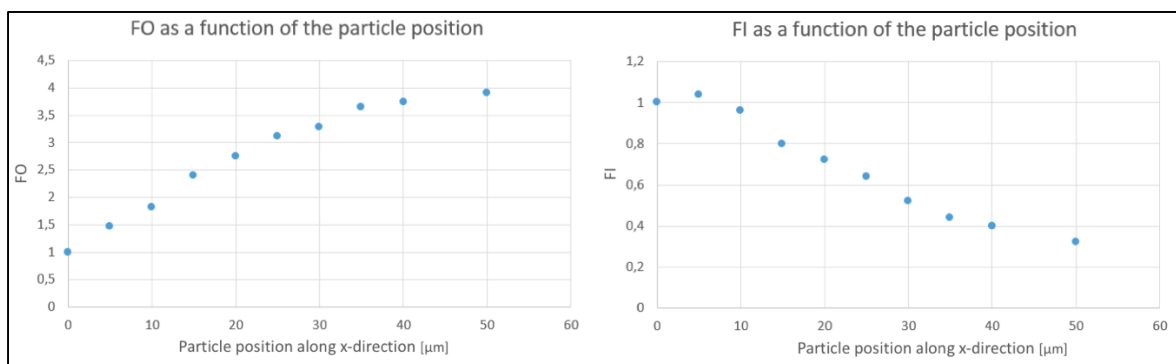
Supplementary Figure S1. Diagram of the geometry of the model.



Supplementary Figure S2. Velocity field in the $z=0$ plane.



Supplementary Figure S3. Velocity field in the $z=0$ plane for different positions of the trapped particle.



Supplementary Figure S4. Optimal values of F_0 and F_I parameters to keep the particle in equilibrium at different x -positions. The position along the y - and z -direction was kept at $(0,0)$.

2. The effect of the water droplet formed during the experiment on flow resistance.

In the experiments for finding the hydraulic flow resistance of the microfluidic channels of the chip, the water used had to be able to exit the setup freely. Consequently, this led to a droplet developing over the place where the water exited the chip. This droplet would also increase in volume as more fluid was led through the microfluidic chip during the experiments. To evaluate the influence that the water droplet had on the the experimental results follows here the numerical calculations that were employed to estimate the size and the evolution of the overpressure that the water droplet contributed to the experiment with.

When the water in the experiments exits the chip, an interphase is created between the water and the surrounding atmospheric air. Due to this interphase, an overpressure is developed inside the droplet compared to the outside. This overpressure can be defined as the pressure difference, Δp , also referred to as the Laplace pressure, between the inside pressure, p_{in} , and the outside pressure, p_{out} , of the droplet. For a droplet the Laplace pressure is dependent on the surface tension of the liquid and the radius of the (see figure S5). For spherical shapes, the Laplace pressure is related to the surface tension, σ , and the radius, R , of the curvature of the droplet, by:

$$\Delta p = \frac{2\sigma}{R}$$

The surface tension of water at 20°C is $\sigma = 72.5 \cdot 10^{-3}$ N/m. If we consider a droplet of 3 mm in radius, the overpressure inside the droplet will be:

$$\Delta p = \frac{2 \cdot 72.5 \cdot 10^{-3}}{3 \cdot 10^{-3}} = 48.3 \frac{\text{N}}{\text{m}^2} = 0.48 \text{ mbar}$$

So, the overpressure formed inside a 3 mm droplet is small compared to the pressures applied during the experiment. Another thing to consider is that the droplet will change in volume, as liquid will exit from the chip into the droplet as the experiments are carried out. Although the contact angle between PDMS and water is about 105°, which means that the water droplet will not take the shape of an an exact semisphere, it will anyway, from here on, be considered as a half sphere in order to simplify the calculations. So, considering a flow rate of 7 $\mu\text{l}/\text{min}$ ($7 \cdot 10^{-9}$ m^3/min) and a semispherical droplet with the volume, V , the rate of change of the radius of the sphere will be:

$$V = \frac{1}{2} \left(\frac{4}{3} \pi R^3 \right)$$

$$\frac{\partial V}{\partial t} = \frac{1}{2} 4\pi R^2 \frac{\partial R}{\partial t} = 7 \cdot 10^{-9} \frac{\text{m}^3}{\text{min}}$$

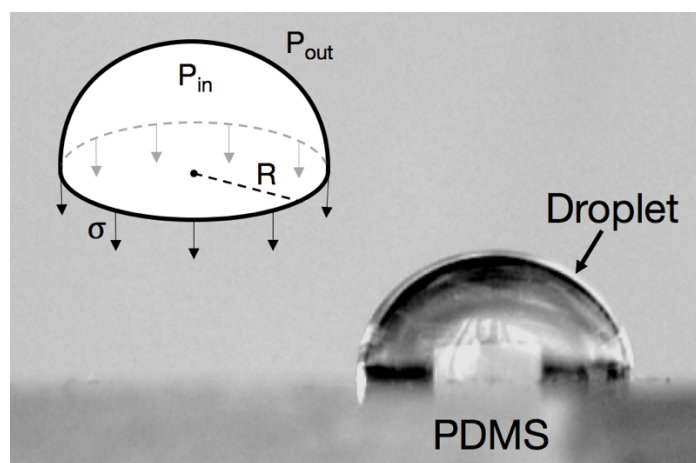
$$\frac{\partial R}{\partial t} = \frac{2 \cdot 7 \cdot 10^{-9}}{4\pi R^2} = 1.2 \cdot 10^{-4} \text{ m/min}$$

This makes it possible to determine the rate of change of the overpressure:

$$\Delta p = \frac{2\sigma}{R}$$

$$\frac{\partial \Delta p}{\partial t} = \frac{\partial \Delta p}{\partial R} \frac{\partial R}{\partial t} = \frac{2\sigma}{R^2} 1.2 \cdot 10^{-4} = 2 \frac{\text{N}/\text{m}^2}{\text{min}} = 0.02 \text{ mbar}/\text{min}$$

With these calculations, it can be concluded that the effect of the droplet overpressure is not important in experimental measurements, both in terms of absolute value and in terms of variation over time. For future experiments like this, it could also be a possibility to submerge the microfluidic chip under water, e.g. in a petri dish, as that could effectively neutralise the droplet effect.



Supplementary Figure S5. Geometry of water droplet formed on PDMS.

3. The Autofluidics software

Some of the work carried out in this project required special ways of controlling the pressures that were applied to the channels of the microfluidic chip. No available software could easily accommodate this and therefore a custom-made software, Autofluidics, had to be developed. Starting from scratch with it, it took a large amount of work to build it, however it has been an essential tool for performing various experiments and has also been critical for reaching the important milestone of making a platform that automatically can confine a microparticle in free solution. Autofluidics was built with LabVIEW and consists of several modules.

Video feed module

The video feed module was included in order to obtain video of the particle and to convert the behaviour and characteristics of it into a signal that can be interpreted digitally (see figure S6). Although noise and false signals can appear in the binary video, which can be problematic when trying to track a particle, Autofluidics is able to discard these effects (see figure S7).

Hardware connection module

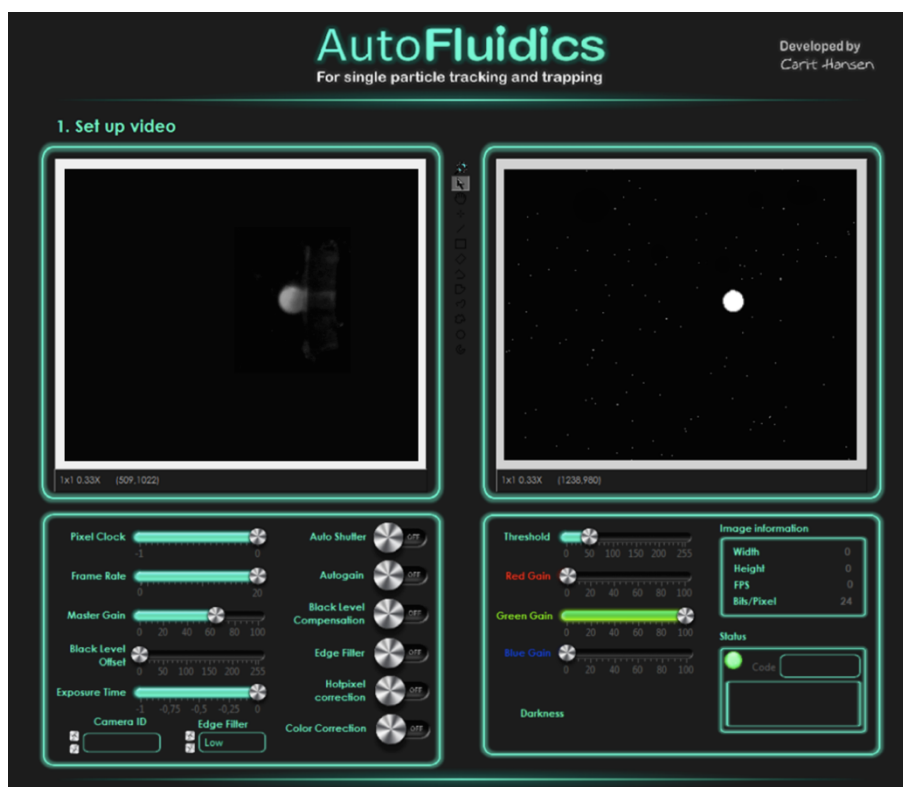
Incorporating a virtual instrument from Elveflow allows Autofluidics to control the OB1 Mk3 pressure controller. Once a USB cable connects the computer to the pressure controller, the connection can be activated by the push of a button (see figure S8).

Pressure control module

The module for controlling the pressure controller can be operated in 8 different modes for different purposes. The mode of operation can be selected from a drop down list (see figure S9A). All modes can be used to adjust the four pressure channels statically, while “Manual” mode also offers the possibility to apply a pressure to channel x_2 that varies according to an amendable sinus curve (see figure S10. Note that in the software the pressure applied to channel x_2 is displayed with yellow digits). In “Confine” there is an opportunity to adjust the pressures in channels x_2 and y_1 according the settings in the feedback module (see figure S11). The software can also be setup to automatically change between modes in a cycle at defined intervals (see figure S9B).

Feedback module

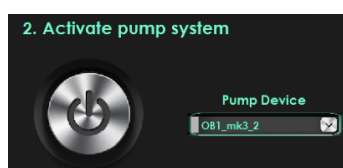
As also displayed in figure 4 of the main paper, the feedback module (see figure S11) is the important module that assess the particle position, based on the digital information generated in the video module (see figure S6) and compares it with the defined confinement area (see figure S10). If the particle is found to be outside the confinement area when the system is operated in “Confine” mode, the feedback will modify the pressures applied by the pressure controller, based on the settings in the feedback module.



Supplementary Figure S6. The setup module involved in converting the video feed signal (upper left box, greyscale) from the uc400 camera into a binary video signal (upper right box, black and white). The binary video feed is dependent on the light intensity of the original video feed. Sliders for controlling the intensity of different colours and a slider for adjusting the cut-off of the minimum required intensity (lower right box) are useful for improving the quality of the binary video.



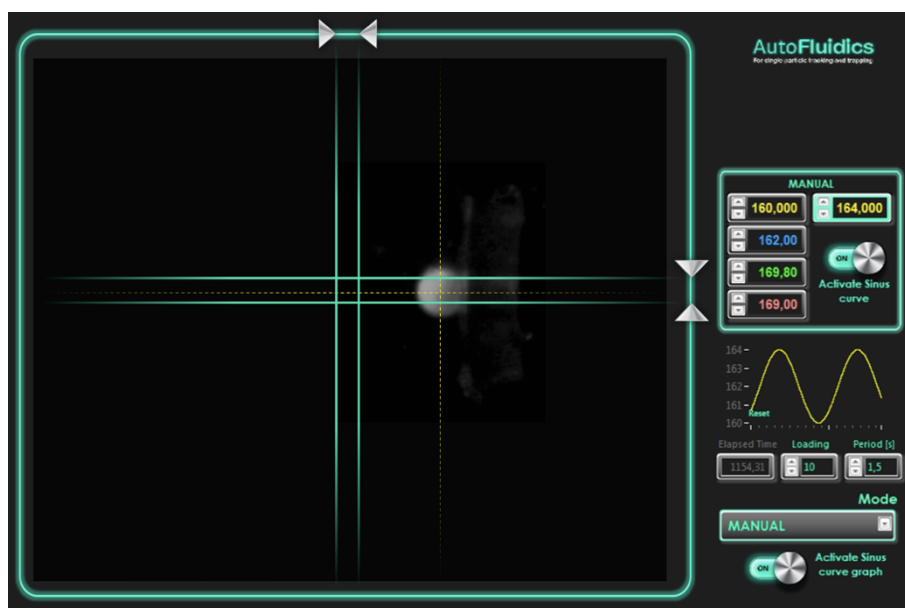
Supplementary Figure S7. Module for identifying a particle from non-particle signals. Left box shows a list of signals present in the binary video in a snapshot of time, with information given on the area of each signal (i.e. number of pixels in a cluster) (right column) and the centre of each signal in x- and y-directions (left and right columns respectively). Right box shows an ordered list of the signals from the left box that are above the threshold value that can be defined in the box below.



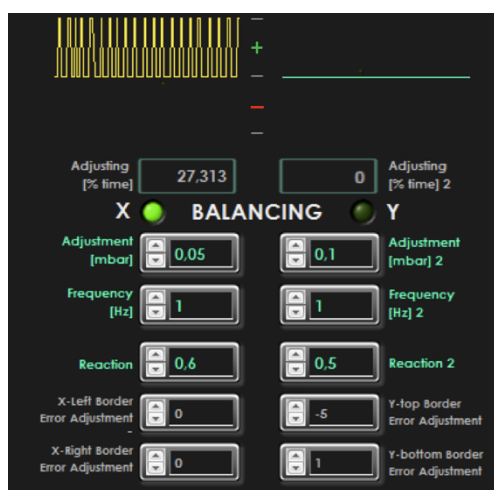
Supplementary Figure S8. The setup module for establishing a connection to pressure controlling equipment.



Supplementary Figure S9. Different modes of controlling the pressures applied to the microfluidic chip by the pressure controller. A) Drop-down list for mode selection. B) Display of all of the available operation modes, with only “Manual” mode not present. Pressure values can be defined for all of the operation modes at any time. When “Cycle” mode is chosen, the operation mode will change between the modes numbered 1 to 6, where each mode will run for the period of time that has been set in the box below it.



Supplementary Figure S10. Video feed with a graphical overlay that locates the centre of the particle and makes it possible to define the borders of a desired confinement area.



Supplementary Figure S11. The feedback module assesses the position of the particle relatively to the set borders of the desired confinement area. When “Confine” mode is selected, the feedback will alter the pressures in up to two of the channels if the particle is not inside the defined confinement area. In this module it is possible to modify the intensity and the responsiveness of the pressure adjustments.